Energy 192 (2020) 116609

Contents lists available at ScienceDirect

Energy

journal homepage: www.elsevier.com/locate/energy

Impact of long-term resource variations on wave energy Farms: The Icelandic case

Markel Penalba [a, *], Alain Ulazia [b], Jon Saénz [c, d], John V. Ringwood [e]

[a] Department of Mechanical and Manufacturing, Mondragon University, Loramendi 4 Apdo. 23, 20500, Arrasate, Spain
[b] Department of NE and Fluid Mechanics, University of the Basque Country (UPV/EHU), Otaola 29, 20600, Eibar, Spain
[c] Department of Applied Physics II, University of the Basque Country (UPV/EHU), B. Sarriena s/n, 48940, Leioa, Spain
[d] Joint Research Unit (UPV/EHU-IEO) Plentziako Itsas Estazioa, University of Basque Country (UPV/EHU), Areatza Hiribidea 47, 48620, Plentzia, Spain
[e] Centre for Ocean Energy Research, Maynooth University, Maynooth, Co., Kildare, Ireland

ARTICLE INFO

Article history:
Received 19 August 2019
Received in revised form
20 October 2019
Accepted 22 November 2019
Available online 26 November 2019

Keywords:
Wave energy trends
Reanalysis wave data
Teleconnection patterns
Wave energy converters
Wave energy arrays

ABSTRACT

Four decades (between 1979 and 2018) of the wave energy resource around Iceland are analysed in the present paper via the *ERA5* reanalysis, the newest reanalysis of the *European Centre for Medium-Range Weather Forecasts*. While the overall long-term wave trend observed is unremarkable, particularly between the last two decades, in the northern area, near Greenland, a substantial increase of the wave energy resource is detected. In addition, an exceptional decade (between 1989 and 1998) with an extraordinarily high wave energy resource (increasing over 15% with respect to the previous decade) is observed, which emerges due to high values of the indices corresponding to teleconnection patterns, such as the Arctic Oscillation or the East Atlantic pattern. This increase of the total wave energy resource results in more frequent extreme events (up to 35% of the total resource) and, as a consequence, the exploitable wave energy (excluding these extreme events) does not increase proportionally. However, a substantial impact on WEC average power generation is observed, with over 500 kW of difference between two subsequent decades in a WEC farm of 45 devices, meaning that the analysis of long-term resource variations is crucial for an accurate design of different components in the WEC farm.

1. Introduction

Climatic emergency is undoubtedly one of the greatest challenges to mankind for the next decades. The recent report by the Intergovernmental Panel for Climate Change (IPCC) warned that urgent and unprecedented actions are needed to keep the global temperature increase between 1.5 °C and 2 °C. Some of the most significant impacts of climate change are more frequent and powerful extreme events, such as storms, drought, floods, and extreme heat and cold temperatures [1]. In fact, scientists have warned that additional increases in global temperature will significantly worsen these effects [1]. Therefore, a drastic transformation that reconsiders the foundations of the world's economic, social and political systems is crucial, creating a truly sustainable system that minimises the impact of human civilisation on the Earth's ecosystem.

Decarbonisation of the energy sector is found to be the most pivotal action in the way towards a sustainable system due to its higher impact on greenhouse gas emissions (GHGEs): About two-thirds of all the GHGEs stem from the energy sector [2]. In order to gradually increase the renewable share of total energy supply, towards the goal of a 100% renewable energy system that would also have important socio-economic benefits [3], diversification of energy sources is essential. Therefore, less conventional or less developed technologies, such as offshore wind, tidal and wave energy, will also play an important role [4]. Indeed, tidal and, particularly, wave energy are highly promising resources, due to their significantly higher concentration and predictability [5]. Apart from energy generation, wave energy converters (WECs) can also be used for desalination [6], coastal protection [7,8] or flooding mitigation [9], applications that will become essential in the future due to the effects of climate change. In fact, future wave energy farms may be designed for multiple purposes, such as electricity generation and coastal protection [10,11].

Regardless of the application, once WECs become mature and

* Corresponding author.
E-mail addresses: mpenalba@mondragon.edu (M. Penalba), alain.ulazia@ehu.eus (A. Ulazia), jon.saenz@ehu.eus (J. Saénz), john.ringwood@mu.ie (J.V. Ringwood).

https://doi.org/10.1016/j.energy.2019.116609
0360-5442/

achieve commercial viability, an accurate characterisation of the resource at the location where a WEC or a farm of WECs is planned to be installed will be crucial. The characterisation of the resource for a specific location is often presented by means of a scatter diagram, which is created using only measurements of the previous years/decades [12]. These scatter diagrams illustrate the frequency of different sea-states as a function of peak period (T_p) and significant wave height (H_s). However, characterisation of the resource only based on past data can be inaccurate, since potential variations of the resource in the period where the WEC or the WEC farm is supposed to operate are neglected. In that case, WECs or WEC farms designed using these scatter diagrams would be designed for the past resource, but might be potentially sub-optimal in the future resource.

1.1. Wave trends in the literature

The characterisation of the future resource requires an accurate understanding of the wave trends. To that end, the World Meteorological Organisation [13,14] recommends using at least 30 years of data to obtain a reliable estimate of climate variables. Different techniques have been used in the literature for the collection of this data, such as buoy measurements [15], observations from ships [16,17], satellite altimetry [18,19] or numerical models and reanalysis datasets [20–27].

A method which uses the reanalysis datasets is used in the present study, and different reanalyses prepared by the *European Centre for Medium-Range Weather Forecasts* (ECMWF), which can be applied in different cases and are further described in Section 2, are compared in order to select the most appropriate one. Zheng et al. [25,27] present a global wave energy resource study via the *ERA40* reanalysis and another global study of the wave energy resource is presented in Ref. [26].

Wave trends have also been studied in the literature using similar methods, although focusing on wave height in the vast majority of studies [16,17,19,28–30]. Hence, the variations in wave period have usually been neglected, with very few exceptions such as [31,32]. The North Atlantic Ocean, for example, has been studied using different techniques, such as satellite-retrieved data [19], in-situ measurements [28], and visual observations [16,17,29], observing a positive wave height trend of about 5 cm/decade with all the different techniques.

The focus of researchers on wave height is understandable, given the applications those studies were designed for in sectors like navigation, or oil&gas. However, wave period (or frequency) has a key role in the design of WECs and even WEC control strategies, since WECs are typically tuned to resonate with the incoming sea waves. Very few studies that analyse wave period variations can be found in the literature: wave period trends are analysed in Ref. [31], while [32] studies the evolution of peak period and wave height all over the world. Satellite data is also used for estimation of the mean wave period [33–36]. However, the period of time that can be covered using satellite data, compared to other techniques, is very limited, since satellite observations before 2005 are considered unreliable [33]. Therefore, this technique is not appropriate yet for the analysis of historical wave trends. Other studies that also consider wave height, period and directionality over several decades are presented in the literature [37,38]. These studies focus purely on assessment of the resource within a relatively high spatio-temporal and a small study area.

In addition, when analysing variations in the wave energy resource, only seasonal and inter-annual variations, which are reasonably well studied within the last decade [39–42[93]], are studied, neglecting other longer-term variations.

Very little attention has been paid in the literature to these long-term wave trends and, especially, their implications on the design and operation of WECs. Previous studies by the same authors show the relevance of these wave trends in different locations [43–46], demonstrating the significant increase of the wave energy resource and, especially, extreme events, which can be attributed to the effects of climate change. In fact, a more recent study [47] also identifies similar wave trends, where the increase in wave power is found over the 20th century, and links this power increase with climate change, more specifically with oceanic warming.

Finally, other teleconnection patterns, such as the North Atlantic Oscillation (NAO) or the Artic Oscillation (AO), can also have an important impact on the behaviour of WECs. In fact [26], studies the monthly correlation of wave energy with climate indexes, where the NAO, the Scandinavian index (SCA) and the East Atlantic Pattern (EA) present the strongest influence on Atlantic wave power [48]. The influence of the NAO on the variation of the swell is also studied in Refs. [49,50]. Indeed, recent studies suggest that the risk of domino effects of tipping points, which may produce cascading regime shifts that can lead to large changes in the ecosystem, may be greater than expected due to climate change [51].

1.2. Design of WEC farms

The design of ocean energy farms (OEFs), including offshore wind, tidal and wave energy, involves several different aspects [52] and stakeholders [53]. Once the technology and the specific prototype to be deployed are determined, the location of the OEF must be selected based on its bathymetry characteristics and energy potential of the location, where wave-trends should also be considered. The second stage involves optimisation of the layout of the OEF, including the hydrodynamic performance, the station keeping system and transmission network. The final stage involves the development of a plan for the installation, maintenance and decommissioning of the OEF.

However, in order to simplify the analysis, only the hydrodynamic behaviour of WECs is considered in this paper. Several studies have analysed the layout of wave energy farms based only on the hydrodynamic interaction among the devices within the farm. For example [54], studies WEC farms of different sizes by calculating the annual mean power production (AMPP) directly computing the hydrodynamic coefficients for the complete array with a boundary element method (BEM) solver. Different semi-analytical methods have also been suggested to efficiently compute the hydrodynamic interactions within WEC arrays, such as the plain-wave method or the multiple scattering method introduced in Refs. [55,56], respectively. Another alternative is the direct matrix method presented in Ref. [57].

Other more recent studies, for example [58,59], also consider wave directionality in layout optimisation, while [60], based on the hydrodynamic model recently presented in Ref. [61], incorporates six different parameters into the optimisation algorithm. Chowdhury [62] presents an overview of the different methods to analyse WEC arrays and a full section is given to WEC array modelling techniques in Ref. [63].

In any case, the present paper focuses on the study of long-term wave resource variations and their impact on the hydrodynamic behaviour of WEC farms, and, thus, layout optimisation is beyond the scope of the present study.

The remainder of the paper is as follows: Section 2 presents the data and the methodology used in the paper for the study of wave trends, Section 3 describes the hydrodynamic model employed to evaluate the power absorption of the WEC farms, Section 4 introduces the case study, Section 5 shows the results related to resource variations and the power absorbed by the different WEC farms, Section 6 discusses these results and suggests future lines of

research, and Section 7 presents the main conclusions.

2. Wave and atmospheric data

Reanalyses assimilate data of historical observations to provide a global description of the recent (past century) climate. The ECMWF offers different options that are currently available, each of which has different characteristics. Three reanalyses are compared in the validation against buoy data:

- *ERA20C* (henceforth *ERA20*) is a reanalysis of the 20th century that includes data between 1900 and 2010 [64].
- *ERA-Interim* (denoted *ERAI* in the following) is a global reanalysis updated every month and contains data since 1979 [65] but its production has been discontinued in 2019.
- *ERA5* is the most recent dataset of the ECMWF and will cover from the second half of the 20th century (1950) until present [66], although currently the data are available from 1979 onwards.

Each of these datasets are employed in the literature for different applications, depending on the geographical location, spatial- and time-resolution requirements, time period to be covered, or the accuracy required for the study. Table 1 summarises the most relevant information for each reanalysis.

2.1. Wave data

The selected reanalysis is the *ERA5*, for which the main improvements with respect to its predecessors are a much higher spatial and temporal resolution, and a more consistent sea surface temperature and sea ice model. The data generated using the *ERA5* reanalysis is validated against buoy measurements collected in the area of interest. Measurements from a point on the Icelandic coast are available from the Pangaea project (PANG) [67], as illustrated in Fig. 1, and the other wave-measuring buoy selected for validation is the M1 buoy, near the Irish shore, operated by Foras Na Mara (the Irish Marine Institute) [68]. The area with orange sloped stripes represents the area of study where the decadal analysis of wave energy is focused on. Vik village in the South of Iceland is also highlighted on the map due to its advantageous wave energy potential, as shown later in Section 5.1. Indeed, a future WEC farm is more likely to be located close to the shore in order to reduce the cost of electrical connections and maintenance operations.

Table 2 presents the main information (longitude and latitude of the buoys, the nearest gridpoint in the reanalysis grid and the period used for the validation of the reanalysis dataset) of the two buoys, PANG and M1.

2.2. Atmospheric data and teleconnection indices

In order to explain the role played by atmospheric teleconnection patterns in the changes observed in the WEF, three-hourly mean sea level pressure data have been retrieved from

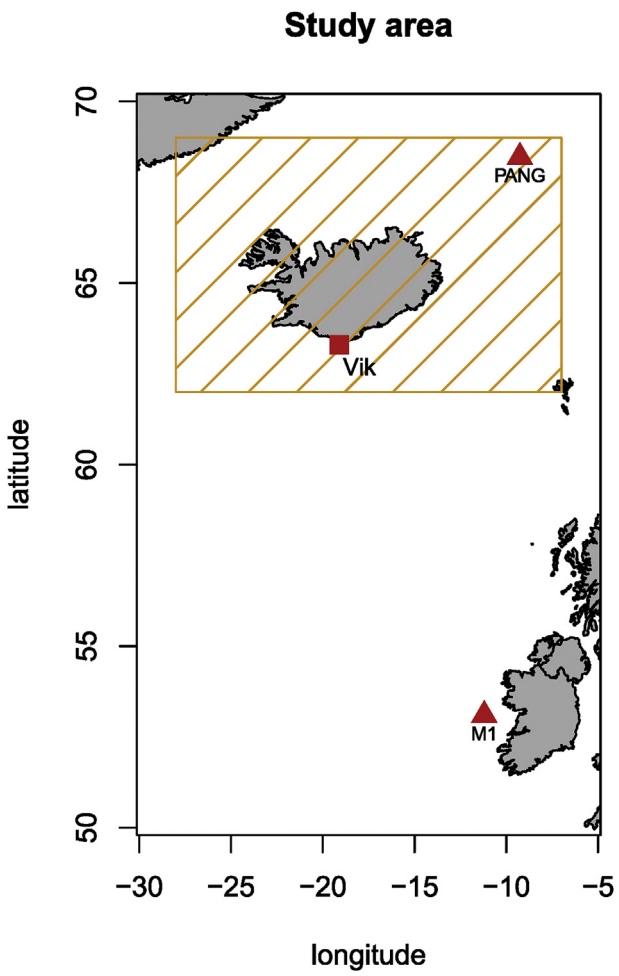

Fig. 1. Location of the wave-measuring buoys.

Table 2
Main characteristics of the wave-measuring buoys.

Buoy	Location (lon, lat)	Nearest gridpoint (km)	Validation period
PANG	(-9.25, 68.46)	6.5	2007–2009
M1	(-11.2, 53.1)	13.2	2003–2010

ERA5. These three hourly data have been band-pass filtered by means of a Lanczos linear filter [69] which removes all the variability outside the two-ten days, leaving this way the variability associated with extratropical synoptic eddies. Monthly standard deviation of filtered mean sea level pressure is thus used [70]. Additionally, monthly averages of mean sea level pressure have also been computed. The role of synoptic disturbances and the mean flow has been analysed by means of the fraction of variance explained by the indices at each ERA5 grid point and by the linear

Table 1
Characteristics of the three reanalysis by ECMWF.

	Period covered	*Assimilation* method	*Spatial* resolution	*Time* resolution
ERA20	1900–2010	24-h 4D-Var	125 km	3-h
ERAI	1979-08/2019	IFS Cycle 31r2 4D-Var	75 km	6 h
ERA5	1979-today	IFS Cycle 41r2 4D-Var	30 km	1 h

regression of the indices with these fields over the ocean.

The indices corresponding to the atmospheric teleconnection patterns have been downloaded from the Climate Prediction Center web server for the case of the NAO, the EA and the AO. Monthly mean values of these indices are used in the study. For the case of the NAO and EA, the indices are calculated by means of Rotated Principal Component Analysis [71] of monthly Northern Hemispheric geopotential height anomalies of the 500 hPa isobaric surface. In the case of the AO, the index is computed by means of the leading empirical orthogonal function of the monthly geopotential anomaly of the 1000 hPa isobaric surface poleward of 20°N latitude [72]. From the monthly values of the teleconnection indices and the monthly anomalies (period 1979–2018) of H_s, Pearson's correlation coefficient, its statistical significance and the associated regression between the index and the H_s field are computed.

2.3. Computation and validation of the wave energy flux

The wave energy flux (WEF) can be computed directly using the variables provided by the *ERA5* reanalysis as a function of H_s and the energy period (T_e) as follows [73],

$$WEF = 0.49 H_s^2 T_e. \tag{1}$$

However, wave period data collected by wave-measuring buoys is usually given by means of T_p. Therefore, in order to complete the validation between the buoy measurements and the reanalysis data, Equation (1) must be adapted to include T_p, which can be achieved by including a correction factor. In that sense, the Wave Period Ratio (*WPR*), implemented in Refs. [43,44,73], relates the energy and mean periods, T_e and T_m, respectively.

The quality of ERA5 is evaluated by means of three statistical metrics: the root mean square error (RMSE), the Pearson correlation factor, and the standard deviation ratio (SDratio) between the model and the buoy observations. These metrics are illustrated in Taylor diagrams [74], where

1. The RMSE is given by the radius of the arc centered at the point corresponding to the observation,
2. The Pearson correlation coefficient is represented by the angular position of the analysed point over the exterior arc, and
3. The SDratio is represented by the radius of the arc with the centre at the origin.

The reanalyses ERAI, ERA20 and ERA5 are compared against the two buoy measurements, using H_s and the corresponding wave period (T_{02} for M1 and T_m for PANG). The results for each model are given in the form of a cloud of points to consider the swept area at a 95% confidence level. The *ERA5* reanalysis shows a modest improvement in correlation for all the different cases compared to ERAI and ERA2, as illustrated in Fig. 2, where the correlations are around 0.95 for H_s and around 0.8 for the wave periods. However, the improvements in SD and RMSE are significant. As expected, the quality of the reanalyses improves according to its spatial resolution and novelty, *ERA5* being the most refined reanalysis followed by *ERAI* and *ERA20*, respectively.

3. Hydrodynamic modelling

The hydrodynamic model employed in the present paper is based on potential flow theory, where the wave-structure interaction is modelled under the assumption of inviscid fluid, and incompressible and irrotational flow. In addition, linear potential flow theory assumes that body motion is small with respect to the wavelength. The assumptions of linear potential flow theory computes the wave-structure interaction problem via the boundary conditions and Bernoulli's equation in terms of the velocity potential and free surface displacement. Hence, the linear hydrodynamic coefficients of the body can be obtained using a BEM solver, such as NEMOH [75] or WAMIT [76].

3.1. Isolated WEC

Once the linear hydrodynamic coefficients (i.e. hydrostatic stiffness, and radiation added-mass and damping coefficients) are computed in the frequency-domain (FD), the equation of motion is given as follows,

$$-\omega^2(M + A(\omega))\widehat{X} + j\omega(B(\omega) + B_{PTO})\widehat{X} + K_H\widehat{X} = \widehat{F}_e(\omega), \tag{2}$$

where M is the mass, $A(\omega)$ the added-mass, $B(\omega)$ the radiation damping, $\widehat{X}$ the position of the body, ω the wave frequency, K_H the hydrostatic stiffness, B_{PTO} the damping value of the PTO force, $\widehat{F}_e(\omega)$ the excitation force and $j = \sqrt{-1}$. Since a linear system is assumed, if sinusoidal waves are considered, motion is also a sinusoidal function that can be written as a function of time: $x(t) = \mathrm{Re}\,(\widehat{X}e^{j\omega t})$. The same can be applied to the forces. The PTO is modelled as a linear damper, optimising the value of the damping coefficient for each sea-state.

This method is applicable to either regular or irregular waves. The latter represent more realistic waves and can be determined for different sea-states (a given combination of H_s and T_p). Therefore, the power absorption of a WEC, when deployed at a specific location, can be obtained via the AMPP, which is calculated combining the absorbed power P_{ir} and the occurrence frequency of each sea-state of $C(H_s, T_p)$:

$$\langle P_i \rangle = \sum_{(H_s,T_p)} P_{ir} C(H_s, T_p). \tag{3}$$

The accuracy of linear models has been demonstrated to be quite poor under certain circumstances, particularly under the action of an energy maximising control strategy [77], overestimating the motion and power absorption of WECs [78]. The impact of these nonlinear effects varies significantly for different WEC-types [78]. Similarly, the inaccuracy of an excessively simplified PTO model is also demonstrated in the literature [79], where incorporating nonlinear dynamics, constraints, and losses and efficiencies of the different PTO components leads to a significantly lower AMPP. However, the linear hydrodynamic model and the simplified PTO model result in a computationally efficient mathematical model that provides a reasonable approximation for a first estimation of the power production capability of a WEC.

3.2. WEC array

The same linear model presented in Section 3.1 can also be generalised to the array case. In fact, a computationally efficient model is imperative when analysing WEC farms or arrays of several devices, meaning that the characteristics of the linear model are particularly appealing for the analysis of WEC arrays. For the case of N devices in an array, Equation (2) can be easily extended by introducing the matrix notation:

$$-(\tilde{M} + \tilde{A}(\omega))\omega^2\widehat{X} + (\tilde{B}(\omega) + \tilde{B}_{PTO}(\omega))j\omega\widehat{X} + \tilde{K}_H\widehat{X} = \tilde{F}_e(\omega), \tag{4}$$

where $\tilde{A}$ and $\tilde{B}$ are NxN symmetric matrices (N being the number of devices in the array, as a single degree of freedom is considered for each device), $\tilde{M}$ and $\tilde{K}_H$ are diagonal matrices of the same order as $\tilde{A}$

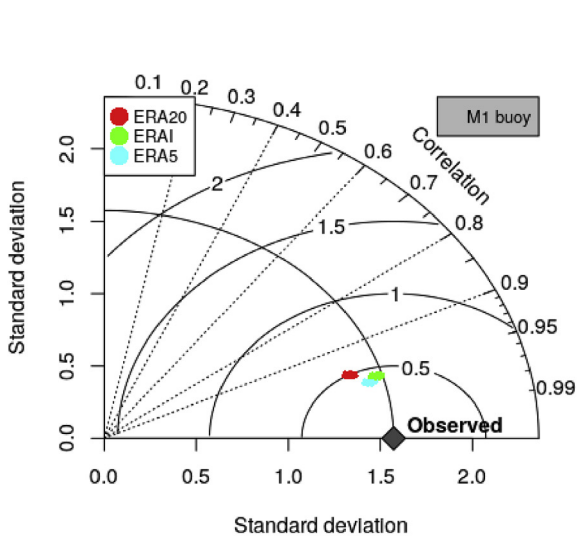

(a) Significant wave height at M1

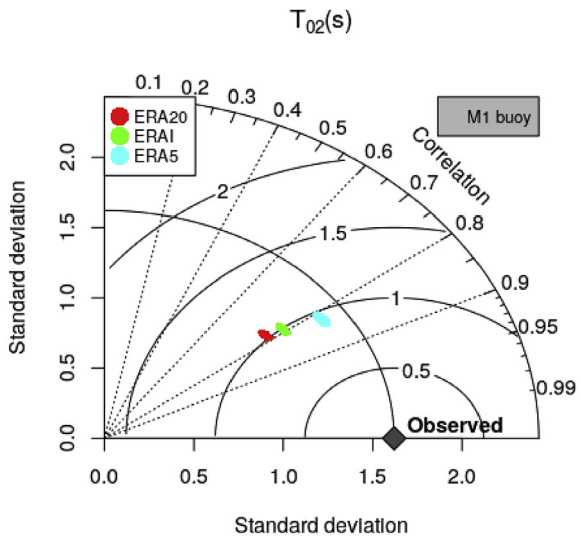

(b) Average zero-crossing period at M1

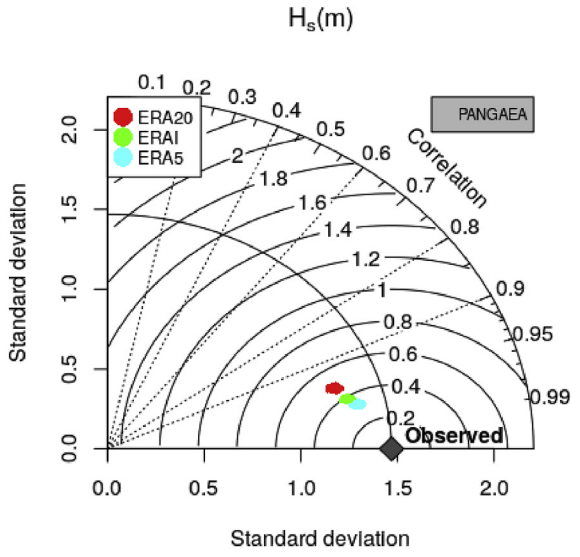

(c) Significant wave height at Pangaea

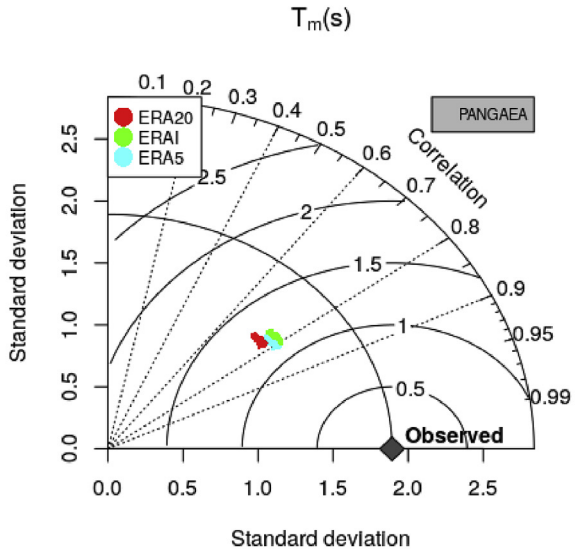

(d) Mean wave period at Pangaea

Fig. 2. Taylor diagrams of wave height and period at the two buoys. ERA5, ERAI and ERA20 are compared.

and $\tilde{B}$, and $\hat{X}$ and $\tilde{F}_e$ are Nx1 vectors. Matrices $\tilde{A}$ and $\tilde{B}$ are symmetric, since off-diagonal values represent two-way hydrodynamic interaction, where the effect of the device i on the device j and vice versa are the same ($a_{ij} = a_{ji}$).

Power absorption of arrays subject to irregular waves is calculated in the same way as for single devices following Equation (3), where the absorbed power (P_{ir}) denotes the power of the whole array. For further details about the hydrodynamic model, the reader is referred to Ref. [54]. This method has previously been used in a variety of studies in the literature [80,81].

4. Case study

4.1. Icelandic Waters

Iceland is a particularly interesting location, for several reasons. Firstly, Iceland is one of the primary examples in the integration of renewable energy sources into the national electricity grid, with almost 80% of its final energy consumption derived from renewable energy sources [82]. In addition, the island has no interconnections with other countries, which makes it completely self reliant. Finally,

Iceland is an island with a long and strong cultural connection with the ocean, which makes marine energy particularly interesting. The Icelandic Waters ecoregion [83] is divided into four main sub-areas, as illustrated in Fig. 3.

Among the four different sub-areas, southern and northern shelves (sub-areas 1 and 2 in Fig. 3) are relatively shallow waters. In contrast, sub-areas 3 and 4 in Fig. 3 are beyond the shelf, where the ocean becomes too deep for the implementation of any marine renewable technology available today. One of the main drawbacks for the installation of marine energy technologies, within the Exclusive Economic Zone (EEZ), is that fishery is one of the most important economic activities of the country.

4.2. Wave energy conversion

4.2.1. Selected wave energy converter

The geometry of the WEC considered for the present study is based on the dimensions of the CETO 6 device, which is a submerged oscillating point absorber that reacts against the seabed, as illustrated in Fig. 4 (a), and harvests the energy from surge and heave motion [84]. The geometry used in the present paper differs slightly from the real CETO device, in the sense that the device used in the analysis is a pure cylinder of 10 m radius and 6 m height.

Using the hydrodynamic model presented in Section 3.1, the power matrix of the isolated WEC can be obtained, illustrating the power that can be absorbed from each sea-state, as shown in Fig. 4 (b). This power matrix shows the power absorption capabilities of the WEC for peak wave periods between 4 and 16 s, and significant wave heights between 0.25 and 10 m. However, the real operational space of the WEC is significantly smaller, since the WEC switches into survival mode in sea-states where the structural integrity of the device is threatened. Therefore, the red line plotted in Fig. 4 (b) illustrates the power production space, beyond which, the device stops producing energy to minimise structural damage.

4.2.2. WEC farm size and layout

WEC farms can be formed by arranging isolated WECs into different configurations. The hydrodynamic behaviour of the WEC farm can vary significantly depending on the layout of the WEC farm. If the inter-device separation is sufficiently large, hydrodynamic interactions are negligible, meaning that the devices within the WEC farm behave as isolated devices. Yet, if this inter-device distance is short, hydrodynamic interaction can reduce the power absorption of the WEC farm mainly due to masking or shadow effects, or increase the power absorption of the WEC farm by taking advantage of the diffracted/radiated waves from the surrounding devices in the farm. These two effects are respectively known as *destructive* and *constructive* interaction.

In any case, since WEC layout optimisation is beyond the scope of this work, a particular fixed configuration is studied. The selected configuration is a staggered configuration, where devices of two consecutive rows in the array are deployed in alternating positions by horizontally displacing one of the two consecutive rows as illustrated in Fig. 5 for an array of 5 devices. In addition, the horizontal (**x**) and vertical (**y**) inter-device spacing (**d**, in Fig. 5) is identical in the arrays used in this paper, and is defined as 20 times the WEC diameter, based on the results presented in Ref. [54].

The staggered configuration minimises the masking or shadow effects that result in significant reductions of the absorbed power, as demonstrated numerically [85] and experimentally [86].

The number of devices in the WEC farm can vary depending on several factors. Therefore, WEC farms of different sizes are analysed in this paper, in order to study the effect of the long-term resource variations on different WEC farms: a small farm, a medium farm and a large farm. Some developers suggest that the future of wave energy is in very large WEC farms, consisting of tens or even hundreds or WECs. However [52], concludes that increasing the number of devices in ocean energy array beyond a certain threshold, does not necessarily reduce the levelised cost of energy (LCOE) of the farm. The study analyses ocean energy arrays of 10, 50

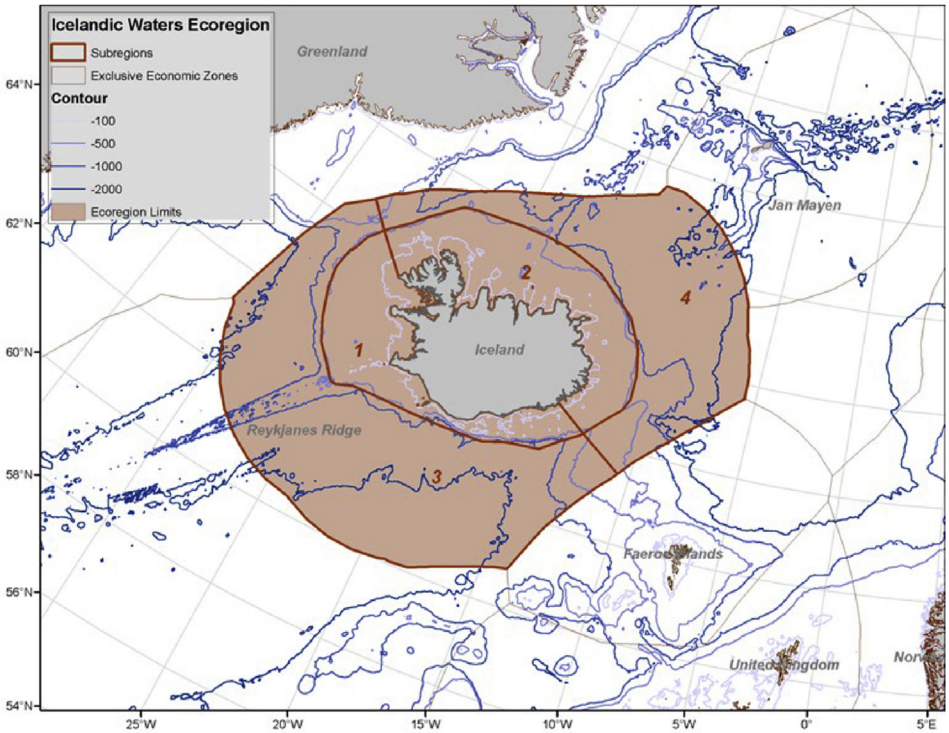

Fig. 3. The Icelandic Waters ecoregion with the different defined EEZs [83].

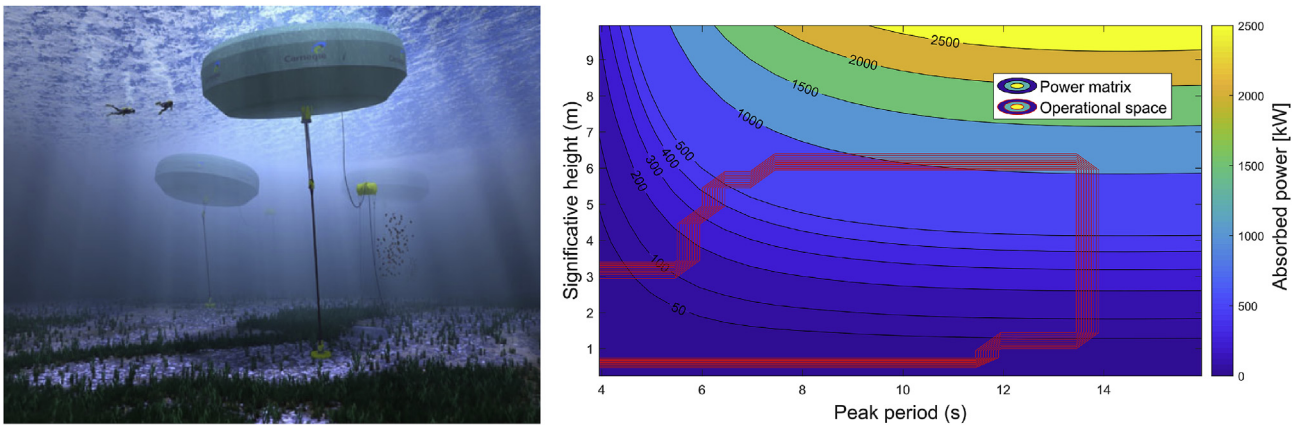

Fig. 4. Wave energy converter: (**a**) Illustration of the CETO 6 prototype [84] and (**b**) the power matrix of the CETO-like WEC employed in this study.

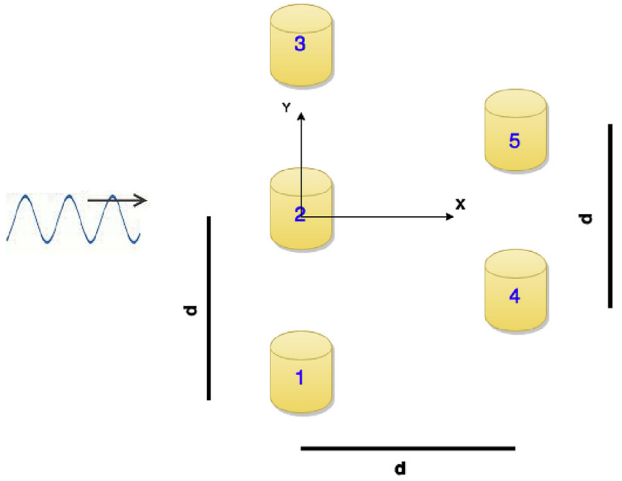

Fig. 5. Illustration of the staggered configuration implemented in this study: an example with 5 devices.

and 100 devices, demonstrating that the farm with 50 devices shows the best figures for the LCOE, the capacity factor and the CAPEX.

Therefore, in this study, small, medium and large farms are formed by 9, 18 and 45 devices, respectively. Table 3 presents the details of the different WEC farms analysed in this study, including the number of devices and the approximate area occupied by the farm.

5. Results

This section is divided into two main parts: Section 5.1 presents the variation of the resource since 1979, while Section 5.2 illustrates the impact of those resource variations on the power production capabilities of the WEC farm.

Table 3
Details of the different WEC farms analysed in this paper.

	Small farm	Medium farm	Large farm
# devices	9	18	45
Occupied area [km^2]	1.6	4.8	14.4

5.1. Wave resource variations

The average values of the historical variation of the wave resource highlight the wave trend in the area of interest for the four decades of the analysis period of ERA5: 1979–1988, 1989–1998, 1999–2008, 2009–2018. These trends are computed via the non-parametric Theil-Sen method [87,88], which fits a line using the median of the slopes. The significance of the trend at each gridpoint is evaluated at a 95% confidence level, using bootstrap re-sampling with 1000 samples.

Hence, wave trends in the present paper are analysed using the following variables:

1. The average H_s, T_m and WEF values for the entire area of study, obtained via the *ERA5* reanalysis. These mean values illustrated in geographical maps (see Fig. 7) provide a general picture of the wave resource, clearly identifying the most energetic locations within the area of study.
2. Decadal average of WEF values over the four decades, calculated using the ERA5 reanalysis. The evolution of these decadal values allows for the identification of the main wave trend, and the changes between decades.

3. Decadal trends of the seasonal WEF for winter. The seasonal analysis gives more information about the distribution of the resource over the year. As expected, it has been found that spring and autumn constitute intermediate cases, and that summer is the less energetic season. Thus, winter shows the most interesting behaviour for the increase of wave energy within these 40 years.

The average values of H_s, T_m and WEF are calculated for all the gridpoints available in the *ERA5* reanalysis within the area of study, the combination of which allows for the constitution of different maps, as shown in Fig. 6 (a)–(c), respectively. These maps illustrate the significant differences among the sub-areas of the Icelandic Waters ecoregion. The southern sub-area presents a promising area for the implementation of WEC farms, with mean H_s and T_m of 3.4 m and 9 s, respectively. In contrast, the resource in the northern sub-area is significantly weaker, where mean H_s and T_m are reduced to 0.3 m and 4.3 s, respectively.

The wave energy resource is proportional to the square of H_s, as shown in Equation (1), and, as a consequence, the WEF is significantly higher in the southern sub-areas, up to 59 kW/m, compared to the northern sub-areas, where the WEF is reduced below 10 kW/m. Therefore, it seems clear that the southern sub-areas are substantially more appealing for the implementation of a WEC farm.

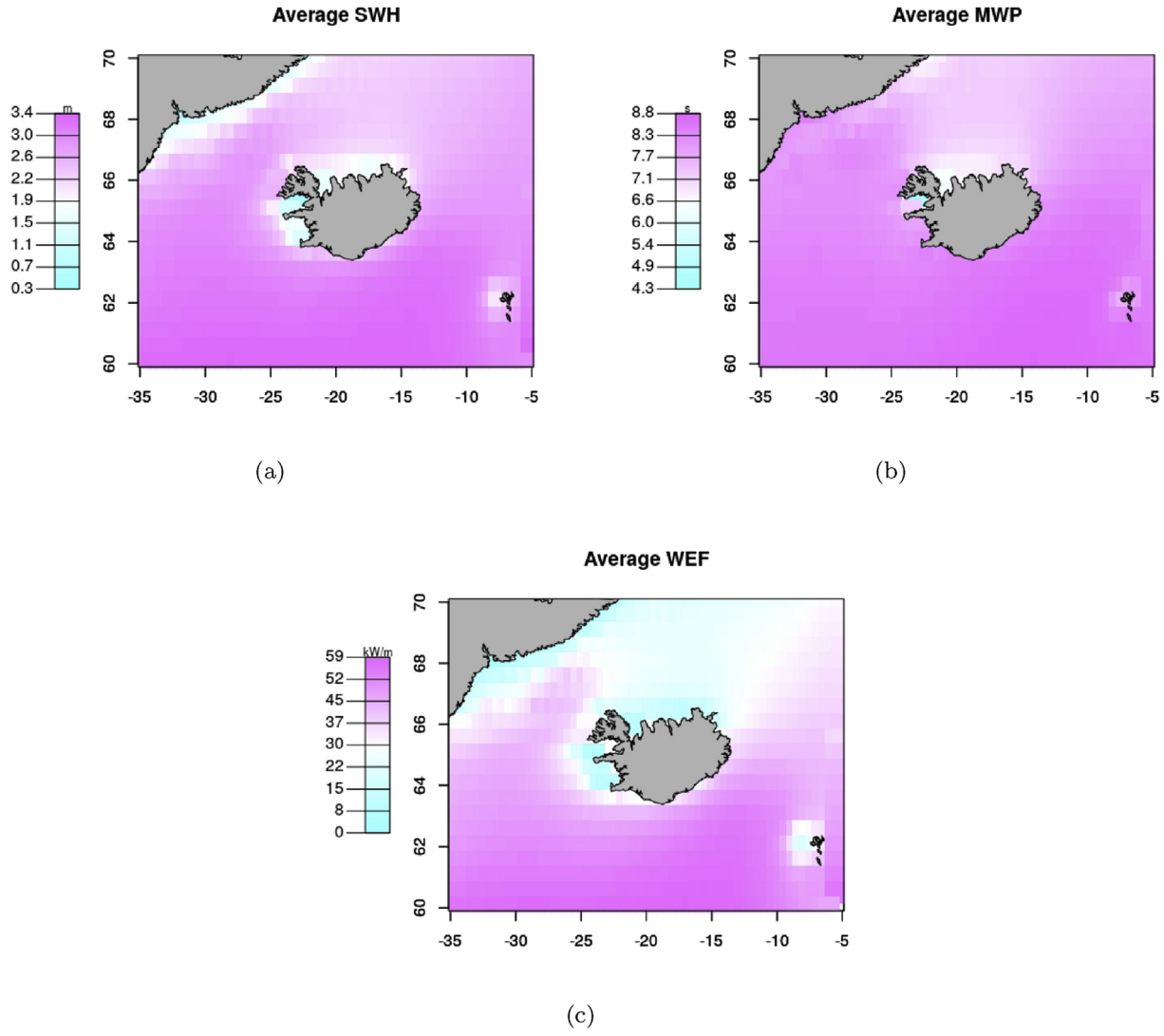

Fig. 6. Mean values of H_s, T_m, and WEF in the study area.

Therefore, the present paper focuses on the area close to the village of Vik in the south of the country, as illustrated in Fig. 1.

Apart from the mean values, the evolution of the wave energy resource over the four decades between 1979 and 2018 provides a better insight into the wave resource in the location under analysis. Fig. 7 shows the evolution of the WEF, where a clear increase is shown between the first and the second decade in Fig. 7 (b), particularly in the northern areas close to Greenland and in the west of the island. The WEF in the southern sub-areas also increases during the second decade, reaching up to 45 kW/m in the areas near the Vik village. In contrast, over the third and fourth decades, between 1999 and 2018, a reduction of the WEF can be observed, returning to the values observed in the first decade, around 40 kW/m. Thus, although a significant increase in WEF occurs from the first to the second decade, the overall long-term wave energy trend during these 40 years is largely neutral.

Although the broad picture is useful in order to understand the resource and the overall wave trend in the region, the design of a WEC farm requires the analysis of a more specific area. Table 4 presents the evolution of the main resource parameters over the four decades at the gridpoint closest to Vik, where the maximum values are always observed in the second decade. The last column in Table 4, showing the maximum H_s values over each decade, is particularly noteworthy, showing an increase (almost 15%) that suggests a significant increase of extreme events within this decade. The mean H_s and T_p values shown in Table 4 also show a significant increase between the first and the second decades, and a less significant decrease during the third and fourth decades.

In order to better understand the wave resource and trend, it is important to analyse the historical seasonal trends too. In fact, previous studies of the authors [45,46] show that these seasonal trends can be even more pronounced than the annual trends, particularly those corresponding to the winter resource. Fig. 8 (a) and (b) show the winter WEF for the first and last decade (1979–1988 and 2009–2018), respectively, illustrating a significant increase in both the southern and northern areas, close to the Greenland coast. Fig. 8 (c) displays the decadal trend in the area of study, where the main difference is observed in the northern areas, with positive trends of up to 8.9 kW/m per decade in some specific locations.

5.2. Impact on energy absorption

The impact of the wave resource variations, presented in Section

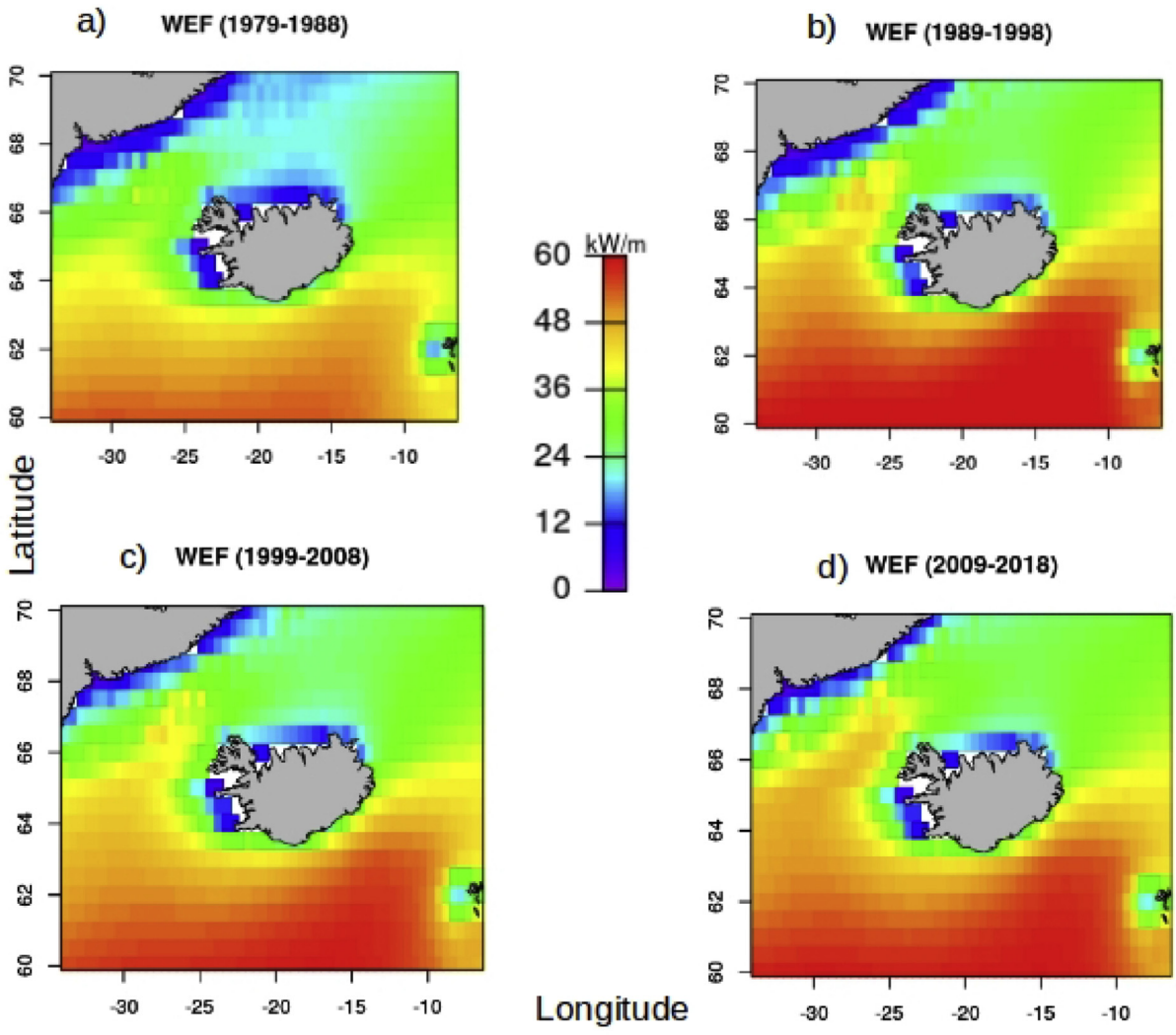

Fig. 7. Mean values of WEF at the four decades of the study period: a) 1979–1988; b) 1989–1998; c) 1999–2008; d) 2009–2018.

Table 4
Wave trend of the resource close to Vik.

Decades	WEF [kW/m]	mean H_s [m]	mean T_p [s]	max. H_s [m]
1979–1988	38.95	2.79	9.91	13.73
1989–1998	45.33	2.97	10.26	15.66
1999–2008	41.20	2.90	10.08	12.45
2009–2018	41.71	2.93	10.14	11.33

5.1, on the power output of the WECs is analysed following the formulation described in Section 3. The impact on the power absorption is evaluated first for an isolated device and then the different WEC farms described in Table 3. It should be recalled that the power production operational space of the WEC, defined in Fig. 4 (b), has a significant impact on power absorption, excluding the most energetic sea-states and extreme events. Fig. 9 (a) and (b) illustrate the total and the exploitable resource (excluding the resource beyond the operational space), and the difference between the two in percentage terms, respectively.

Fig. 9 (a) shows that the WEF is largest in the second decade, but so is the difference between the total and the exploitable resource, which confirms the increase of extreme events, as suggested previously when discussing the results shown in Table 4. In addition, although the total resource over the last two decades reduces to the values observed in the first decade, the exploitable resource is even higher due to the significant reduction of the extreme events observed in Fig. 9 (b).

Such variation in the total and exploitable WEF has an important impact on the AMPP of WECs. Fig. 10 (a) illustrates the AMPP per device of different WEC farms, including the case with only one WEC, for different decades, where differences seem to be rather small (about 5%). The first observation is that hydrodynamic interactions in the WEC farm are relatively weak. Mildly constructive interactions can be observed for small and medium arrays, while mildly destructive interactions appear in the large array. Secondly, Fig. 10 (a) illustrates that the AMPP is largest in the last decade (2008–18), which is the decade that shows the largest exploitable WEF, even if the total WEF is larger in the second decade (1989–88). Therefore, these results may suggest that long-term variations in Iceland have almost no impact on the power production performance of WECs, which might be correct for isolated devices.

However, small differences between the decades in AMPP per device can still have a considerable impact on WEC farms, as shown in Fig. 10 (b). In the case of WEC farms of 9 and 18 devices, the relatively small differences in the AMPP per device result in a maximum difference of about 110 kW and 220 kW, respectively,

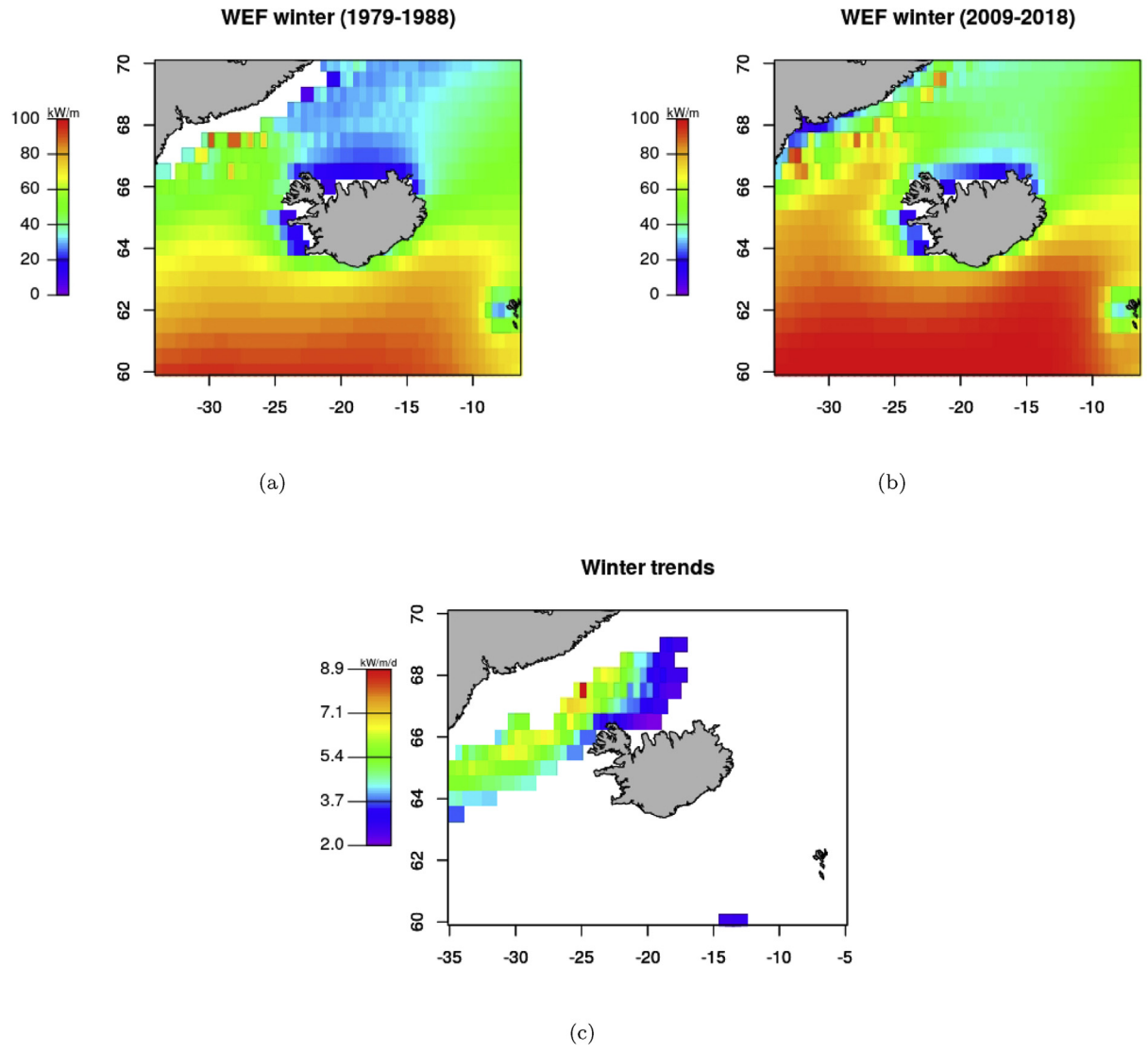

Fig. 8. Mean winter values of WEF at the first decade and the last one and the trends per decade: a) winters of 1979–1988; b) winters of 2009–2018; c) WEF decadal trends for winter that are significant at a 95% confidence level.

between the second and third decades, which means almost 8% of the total power of the farm. Similarly, for a WEC farm with 45 WECs, which is the size that minimises the LCOE and maximises the capacity factor according to Ref. [52], that difference increases to over 510 kW.

6. Discussion

Overall, the analysis of the resource in the ecoregion around Iceland shows a relatively steady resource, especially in the last two decades, as shown in Fig. 7 and Table 4. In contrast to the previous studies of the authors, where wave energy was found to increase significantly in different locations, no significant wave trend was found in Iceland. However, the recent study [47], concerning the variations of the global wave power resource, shows an almost null wave trend around Iceland between 1985 and 2008, which is consistent with the results provided in the present paper.

A relevant wave trend is only found in a specific area of the ecoregion near Greenland. Shaded areas in Fig. 11 illustrate linear regression coefficients with a confidence level of 95%. These shaded areas spread almost all over the Atlantic Ocean in Fig. 11 (a), where regression coefficients are shown to be significantly different from zero. Besides the well known effect of the EA and AO indices in the climate variability of temperate regions [70,89] and, particularly, waves [48], it can be seen that positive phases of the EA index are consistent with an increase of significant wave height to the North of Iceland and Southern Greenland. In order to elucidate whether these variations are associated to wind seas or swell, the analysis has covered both the mean flow (Fig. 11 (a)) and the standard deviation of synoptic perturbations (Fig. 11 (c)). The rationale is that the mean flow, given enough fetch, could produce both higher swell and wind seas, while short-lived and small-scale synoptic perturbations would be expected to produce higher wind seas locally.

Hence, Fig. 11 illustrates that, for the case of the EA index, both effects are detected in the northern part of Iceland. In contrast, the variability of wave height associated to the Arctic Oscillation is tied to the southern facade of Iceland, which is also consistent with the mean flow characteristic of the AO pattern (Fig. 11 (b)). In addition, the impact of the AO on the structure of the Atlantic stromtrack in the north of Iceland cannot be totally excluded, although its effect would, in any case, be weaker than that detected in the trends

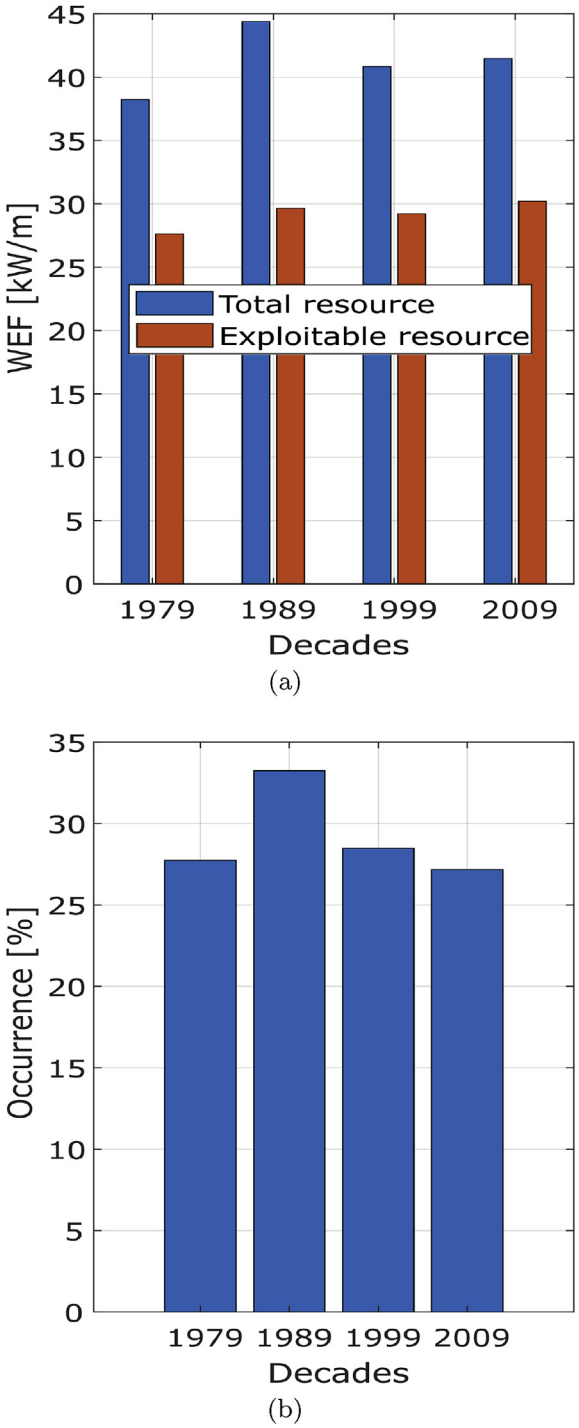

Fig. 9. The exploitable resource: (a) comparison of the total and the exploitable resource, and (b) the occurrence in percentage of the extreme sea-states beyond the operational space defined in Fig. 4 (b).

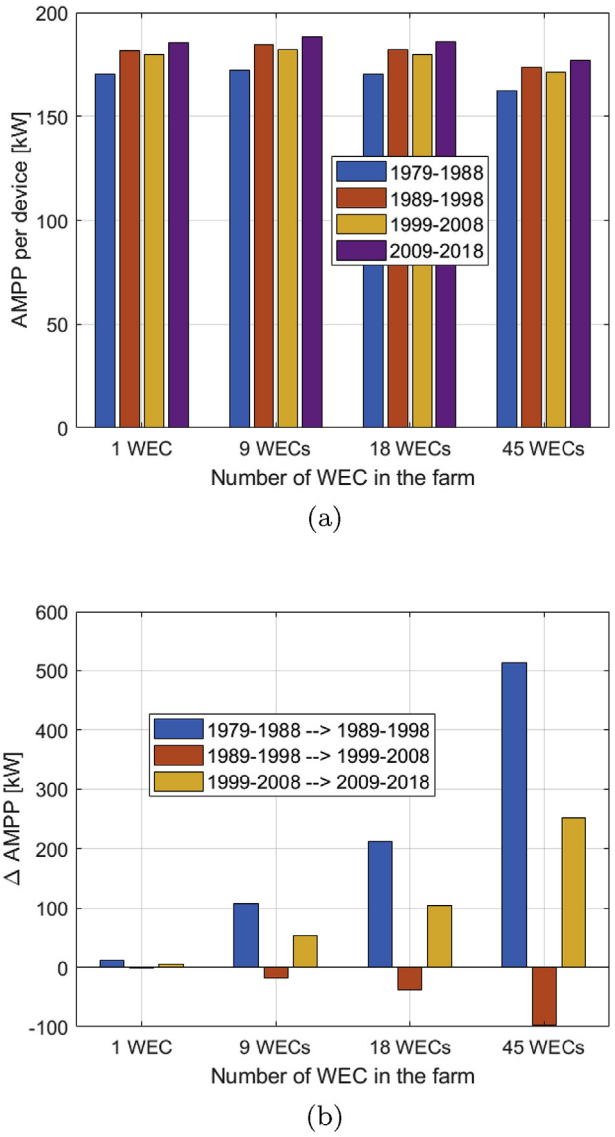

Fig. 10. (a) The AMPP per device and (b) the difference of the total AMPP between decades, for different sizes of WEC arrays.

shown in Fig. 8. This can be explained by the fact that there are decadal changes in the EA index which cannot be detected in the case of the AO index (Fig. 12). A linear trend analysis for the EA index from 1979 to 2018 shows that the positive linear trend is statistically significant to a 95% confidence level, whilst a similar analysis for the AO index yields a result that is not significant to a 95% confidence level.

In addition, an anomaly can be observed in the second decade (between 1988 and 1999): the WEF increases substantially all over the area of study, as illustrated in Fig. 7. This increase is directly connected to the atmospheric variability observed during the 1990s in the North Atlantic Ocean. Previous studies [90,91] have already showed that the high values of the AO index during the first half of the 90s demonstrate that positive phases of the AO and NAO contribute to the increase of the wave energy resource to the south of Iceland. This can also be observed in the results presented in this paper, confirming that the variability associated with the AO index, illustrated on the right map in Fig. 11, is the main reason behind the decadal changes in H_s and, as a consequence, the WEF.

Two main consequences appear as a result of the impact of atmospheric teleconnection patterns on the wave energy resource surrounding Iceland. Primarily, the wave energy resource increases significantly in the area of study, as shown in Fig. 9 (a). On the other hand, extreme events also increase substantially, as illustrated in Fig. 9 (b). Hence, Fig. 9 (a) shows that the final exploitable resource does not increase in proportion to the increase in the total resource. In any case, the exploitable resource increases sufficiently to substantially impact the power generation capability of a relatively

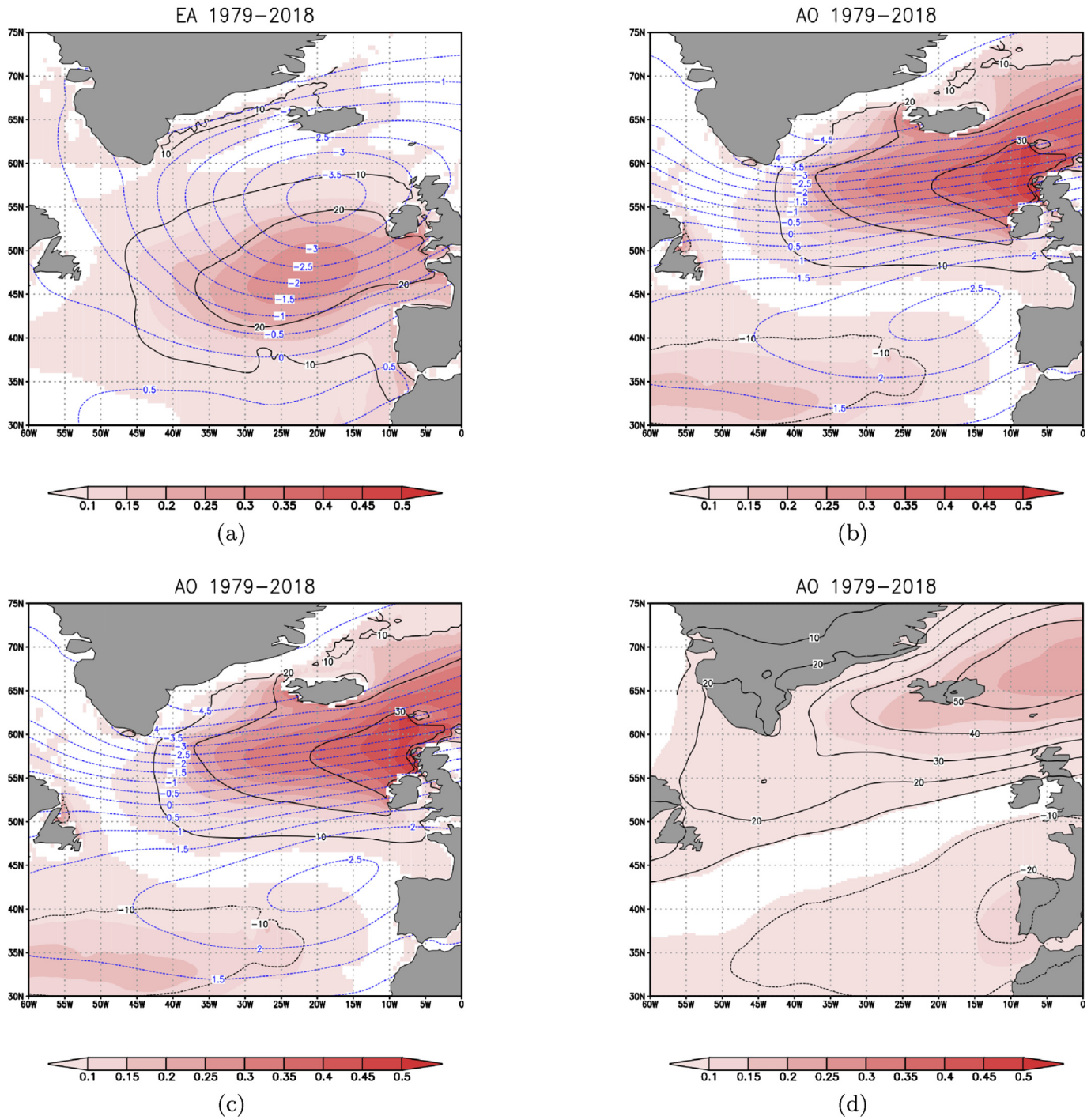

Fig. 11. Squared correlation coefficient illustrated by shaded areas and regression values of H_s with the EA index (a) and AO index (b) illustrated by continuous black lines (in cm), where blue dashed lines represent the regression of the teleconnection indices with mean sea level pressure (in hPa). Fraction of variance (shaded) of the monthly standard deviation of band-pass filtered surface pressure explained by EA (c) and AO (d), and the regression of the indices onto the monthly standard deviation of the filtered pressure (contours). (For interpretation of the references to colour in this figure legend, the reader is referred to the Web version of this article.)

large WEC farm, as illustrated in Fig. 10 (b) (with over 500 kW more power generated every year during the decade). This gain may be relevant for the selection of different components, the design of energy storage systems, electrical cables, and other aspects of a WEC farm.

The variability of wave energy resources associated with these teleconnection patterns may vary in the future due to climate change, as demonstrated for the El Niño phenomenon [92], so that the extraordinary wave energy resources corresponding to the years/decades where the indices of these teleconnection patterns are exceptional, may become the general rule in the future. Therefore, the impact of these teleconnection patterns, through their variation in frequency of occurrence and/or intensity, on the WEC farms of the future may need to be considered for a complete assessment of the wave energy resource (including long-term variations) in the area where a WEC farm is planned to be deployed.

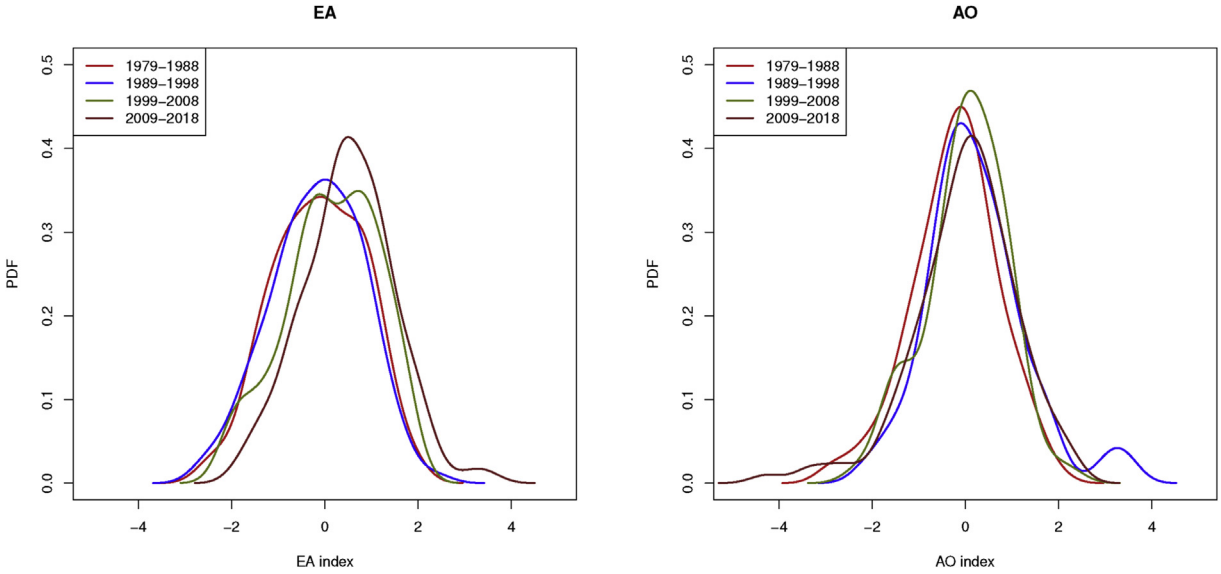

Fig. 12. Decadal variation of the probability density functions derived from monthly values of EA (left) and AO (right) indices.

7. Conclusions

The wave energy resource around Iceland is analysed during four decades between 1979 and 2018. Overall, no relevant wave trend is found, meaning that the wave energy resource in the area of study is maintained relatively constant during the last four decades (about 40 kW/m). However, two more specific phenomena are observed since 1979.

On the one hand, the wave resource in the northern area of Iceland, especially close to Greenland, increases significantly, which can be connected to the positive trend of the East Atlantic Pattern, which induces positive anomalies of wave height near Greenland. On the other hand, the wave energy resource is found to increase substantially within one decade (1989–1998). The latter increase coincides with a period of time where teleconnection patterns, such as Arctic Oscillations or Northern Atlantic Oscillations, were more intense.

These teleconnection patterns increase the total wave energy resource in the area of study, but the exploitable energy (excluding extreme events) does not increase proportionally. However, differences in average power production between two consecutive decades can increase over 500 kW for a relatively large WEC farm (45 devices). Therefore, if long-term resource variations are not considered, in the area where the WEC farm is planned to be deployed, the design of the different components of the WEC farm (energy storage systems, cables and substation for the electrical inter-connections, mooring lines or PTO systems) may be sub-optimal.

Moreover, both the ice mass and the behaviour of teleconnection patterns are likely to be altered due to climate change, meaning that their impact on WEC farms will be more relevant in the future and, as a consequence, the consideration of long-term resource variations is crucial.

Acknowledgements

This research is partly supported by grant CGL2016-76561-R, MINECO/ERDF, UE. Additional funding was received from the University of Basque Country (UPV/EHU, GIU17/002).

References

[1] IPCC. Global warming of 1.5○c. Tech. Rep. Intergovernmental Panel on Climate Change (IPCC); 2018, ISBN 978-92-9169-151-7.
[2] IRENA. Renewable energy: a key climate solution. Tech. Rep. International Renewable Energy Agency; 2017, ISBN 978-92-9260-044-0.
[3] Jacobson MZ, Delucchi MA, Bauer ZA, Goodman SC, Chapman WE, Cameron MA, Bozonnat C, Chobadi L, Clonts HA, Enevoldsen P, Erwin JR, Fobi SN, Goldstrom OK, Hennessy EM, Liu J, Lo J, Meyer CB, Morris SB, Moy KR, ONeill PL, Petkov I, Redfern S, Schucker R, Sontag MA, Wang J, Weiner E, Yachanin AS. 100% clean and renewable wind, water, and sunlight all-sector energy roadmaps for 139 countries of the world. Joule 2017;1(1):108–21. https://doi.org/10.1016/j.joule.2017.07.005.
[4] Weiss CV, Guanche R, Ondiviela B, Castellanos OF, Juanes J. Marine renewable energy potential: a global perspective for offshore wind and wave exploitation. Energy Convers Manag 2018;177:43–54.
[5] Ringwood JV, Bacelli G, Fusco F. Control, forecasting and optimisation for wave energy conversion. IFAC Proc Vol 2014;47(3):7678–89. http://www.eeng.nuim.ie/coer/wp-content/uploads/2017/04/C217JRCT.pdf.
[6] Leijon J, Bostrom C. Freshwater production from the motion of ocean waves - a review. Desalination 2018;435:161–71. https://doi.org/10.1016/j.desal.2017.10.049. desalination using Renewable Energy, http://www.sciencedirect.com/science/article/pii/S0011916417314455.
[7] Abanades J, Greaves D, Iglesias G. Coastal defence through wave farms. Coast Eng 2014;91:299–307. https://doi.org/10.1016/j.coastaleng.2014.06.009. http://www.sciencedirect.com/science/article/pii/S0378383914001306.
[8] Zanuttigh B, Angelelli E. Experimental investigation of floating wave energy converters for coastal protection purpose. Coast Eng 2013;80:148–59. https://doi.org/10.1016/j.coastaleng.2012.11.007. http://www.sciencedirect.com/science/article/pii/S0378383912001809.
[9] Bergillos RJ, Rodriguez-Delgado C, Allen J, Iglesias G. Wave energy converter geometry for coastal flooding mitigation. Sci Total Environ 2019;668:1232–41. https://doi.org/10.1016/j.scitotenv.2019.03.022. http://www.sciencedirect.com/science/article/pii/S0048969719310009.
[10] Abanades J, Flor-Blanco G, Flor G, Iglesias G. Dual wave farms for energy production and coastal protection. Ocean Coast Manag 2018;160:18–29. https://doi.org/10.1016/j.ocecoaman.2018.03.038. http://www.sciencedirect.com/science/article/pii/S0964569117310402.
[11] Cascajo R, García E, Quiles E, Correcher A, Morant F. Integration of marine wave energy converters into seaports: a case study in the port of valencia. Energies 2019;12(5):787.
[12] Nielsen K, Pontes T. Generic and site related wave data. OES-IEA; 2010. Final technical report T02-1.1.
[13] WMO. Calculation of monthly and annual 30-year standard normals. WCDP-No. 10. WMO-TD/No. 341. Tech. rep. World Metheorological Organization; 1989.
[14] WMO. The role of climatological normals in a changing climate. WCDMP-61, WMO-TD/1377, Tech. rep. Word Metheorological Organization; 2007.
[15] Ruggiero P, Komar PD, Allan JC. Increasing wave heights and extreme value projections: the wave climate of the US Pacific Northwest. Coast Eng 2010;57(5):539–52.
[16] Gulev SK, Grigorieva V. Last century changes in ocean wind wave height from global visual wave data. Geophys Res Lett 2004;31(24).

[17] Gulev SK, Grigorieva V. Variability of the winter wind waves and swell in the North Atlantic and North Pacific as revealed by the voluntary observing ship data. J Clim 2006;19(21):5667–85.
[18] Woolf DK, Challenor P, Cotton P. Variability and predictability of the North Atlantic wave climate. J Geophys Res: Oceans 2002;107(C10).
[19] Young I, Zieger S, Babanin AV. Global trends in wind speed and wave height. Science 2011;332(6028):451–5.
[20] Sterl A, Komen G, Cotton P. Fifteen years of global wave hindcasts using winds from the European Centre for Medium-Range Weather Forecasts reanalysis: validating the reanalyzed winds and assessing the wave climate. J Geophys Res: Oceans 1998;103(C3):5477–92.
[21] Cox AT, Swail VR. A global wave hindcast over the period 1958-1997- validation and climate assessment. J Geophys Res 2001;106(C2):2313–29.
[22] Wang XL, Zwiers FW, Swail VR. North Atlantic ocean wave climate change scenarios for the twenty-first century. J Clim 2004;17(12):2368–83.
[23] Wang XL, Swail VR. Climate change signal and uncertainty in projections of ocean wave heights. Clim Dyn 2006;26(2–3):109–26.
[24] Bertin X, Prouteau E, Letetrel C. A significant increase in wave height in the north atlantic ocean over the 20th century. Glob Planet Chang 2013;106: 77–83. https://doi.org/10.1016/j.gloplacha.2013.03.009. cited By 37.
[25] Zheng C, Shao L, Shi W, Su Q, Lin G, Li X, Chen X. An assessment of global ocean wave energy resources over the last 45 a. Acta Oceanol Sin 2014;33(1): 92–101. https://doi.org/10.1007/s13131-014-0418-5.
[26] Reguero B, Losada I, Méndez F. A global wave power resource and its seasonal, interannual and long-term variability. Appl Energy 2015;148:366–80. https://doi.org/10.1016/j.apenergy.2015.03.114.
[27] Zheng CW, Wang Q, Li CY. An overview of medium- to long-term predictions of global wave energy resources. Renew Sustain Energy Rev 2017;79: 1492–502. https://doi.org/10.1016/j.rser.2017.05.109.
[28] Bouws E, Jannink D, Komen G. The increasing wave height in the North Atlantic Ocean. Bull Am Meteorol Soc 1996;77(10):2275–7.
[29] Gulev SK, Cotton D, Sterl A. Intercomparison of the North Atlantic wave climatology from voluntary observing ships, satellite data and modelling. Phys Chem Earth 1998;23(5):587–92.
[30] Zheng CW, Li CY. Variation of the wave energy and significant wave height in the China sea and adjacent waters. Renew Sustain Energy Rev 2015;43: 381–7.
[31] Patra A, Bhaskaran PK. Temporal variability in wind–wave climate and its validation with ESSO-NIOT wave atlas for the head Bay of Bengal. Clim Dyn 2016:1–18.
[32] Camus P, Losada IJ, Izaguirre C, Espejo A, Menéndez M, P J. Statistical wave climate projections for coastal impact assessments. Earth's Future 2017;5: 918–33. https://doi.org/10.1002/2017EF000609.
[33] Caires S, Sterl A, Gommenginger C. Global ocean mean wave period data: validation and description. J Geophys Res: Oceans 2005;110:C02003.
[34] Mackay E, Retzler C, Challenor P, Gommenginger C. A parametric model for ocean wave period from ku band altimeter data. J Geophys Res: Oceans 2008;113(C3).
[35] Gommenginger C, Cotton D, Srokosz M, Challenor P. Ocean wave period from satellite altimeters: validation for envisat ra2. In: Proc. Envisat ERS symp.; 2005.
[36] Gommenginger C, Srokosz M, Challenor P, Cotton P. Measuring ocean wave period with satellite altimeters: a simple empirical model. Geophys Res Lett 2003;30(22).
[37] Morim J, Cartwright N, Etemad-Shahidi A, Strauss D, Hemer M. Wave energy resource assessment along the southeast coast of Australia on the basis of a 31-year hindcast. Appl Energy 2016;184:276–97. https://doi.org/10.1016/j.apenergy.2016.09.064. http://www.sciencedirect.com/science/article/pii/S0306261916313666.
[38] Besio G, Mentaschi L, Mazzino A. Wave energy resource assessment in the mediterranean sea on the basis of a 35-year hindcast. Energy 2016;94:50–63. https://doi.org/10.1016/j.energy.2015.10.044. http://www.sciencedirect.com/science/article/pii/S0360544215014127.
[39] Sivaramakrishnan T. Wave power over the indian seas during the southwest monsoon season. Energy 1992;17(6):625–7. https://doi.org/10.1016/0360-5442(92)90098-K. http://www.sciencedirect.com/science/article/pii/036054429290098K.
[40] Jakimaviius D, Kriauinien J, arauskien D. Assessment of wave climate and energy resources in the baltic sea nearshore (Lithuanian territorial water). Oceanologia; 2017. https://doi.org/10.1016/j.oceano.2017.10.004. http://www.sciencedirect.com/science/article/pii/S0078323417300982.
[41] Wojtysiak K, Herman A, Moskalik M. Wind wave climate of west spitsbergen: seasonal variability and extreme events. Oceanologia; 2018. https://doi.org/10.1016/j.oceano.2018.01.002. http://www.sciencedirect.com/science/article/pii/S0078323418300290.
[42] Ibrahim B, Mahmoud S, Alaraj B. Seasonal sea wave energy at al-manara station in tartous, Energy Procedia 19. In: Alternative Energy as an ultimate solution for the environment of the Mediterranean countries; 2012. p. 104–8. https://doi.org/10.1016/j.egypro.2012.05.190. http://www.sciencedirect.com/science/article/pii/S1876610212009605.
[43] Ulazia A, Penalba M, Ibarra-Berastegi G, Saenz J. Wave energy trends over the Bay of Biscay and the consequences for wave energy converters. Energy 2017;141(C):624–34.
[44] Penalba M, Ulazia A, Ibarra-Berastegui G, Ringwood J, Sáenz J. Wave energy resource variation off the west coast of Ireland and its impact on realistic wave energy converters' power absorption. Appl Energy 2018;224:205–19. https://doi.org/10.1016/j.apenergy.2018.04.121. https://www.sciencedirect.com/science/article/pii/S0306261918306895.
[45] Ulazia A, Penalba M, Rabanal A, Ibarra-Berastegi G, Ringwood J, Sáenz J. Historical evolution of the wave resource and energy production off the chilean coast over the 20th century. Energies 2018;11(9):2289.
[46] Ulazia A, Penalba M, Ibarra-Berastegui G, Ringwood J, Sáenz J. Reduction of the capture width of wave energy converters due to long-term seasonal wave energy trends. Renew Sustain Energy Rev 2019;113:109267. https://doi.org/10.1016/j.rser.2019.109267. http://www.sciencedirect.com/science/article/pii/S1364032119304757.
[47] Reguero BG, Losada IJ, Méndez FJ. A recent increase in global wave power as a consequence of oceanic warming. Nat Commun 2019;10.
[48] Cozannet GL, Lecacheux S, Delvallee E, Desramaut N, Oliveros C, Pedreros R. Teleconnection pattern influence on sea-wave climate in the Bay of Biscay. J Clim 2011;24:641–52. https://doi.org/10.1175/2010JCLI3589.1.
[49] Gulev SK, Grigorieva V. Variability of the winter wind waves and swell in the north atlantic and north pacific as revealed by the voluntary observing ship data. J Clim 2006;19(21):5667–85. https://doi.org/10.1175/JCLI3936.1.
[50] Neill SP, Lewis MJ, Hashemi MR, Slater E, Lawrence J, Spall SA. Inter-annual and inter-seasonal variability of the orkney wave power resource. Appl Energy 2014;132:339–48. https://doi.org/10.1016/j.apenergy.2014.07.023. http://www.sciencedirect.com/science/article/pii/S0306261914007041.
[51] Rocha JC, Peterson G, Bodin Ö, Levin S. Cascading regime shifts within and across scales. Science 2018;362(6421):1379–83.
[52] Topper MB, Nava V, Collin AJ, Bould D, Ferri F, Olson SS, Dallman AR, Roberts JD, Ruiz-Minguela P, Jeffrey HF. Reducing variability in the cost of energy of ocean energy arrays. Renew Sustain Energy Rev 2019;112:263–79. https://doi.org/10.1016/j.rser.2019.05.032. http://www.sciencedirect.com/science/article/pii/S1364032119303454.
[53] Babarit A, Bull D, Dykes K, Malins R, Nielsen K, Costello R, Roberts J, Ferreira CB, Kennedy B, Weber J. Stakeholder requirements for commercially successful wave energy converter farms. Renew Energy 2017;113:742–55. https://doi.org/10.1016/j.renene.2017.06.040. http://www.sciencedirect.com/science/article/pii/S0960148117305451.
[54] Penalba M, Touzón I, Lopez-Mendia J, Nava V. A numerical study on the hydrodynamic impact of device slenderness and array size in wave energy farms in realistic wave climates. Ocean Eng 2017;142:224–32.
[55] McIver P. Some hydrodynamic aspects of arrays of wave-energy devices. Appl Ocean Res 1994;16(2):61–9.
[56] Mavrakos S, McIver P. Comparison of methods for computing hydrodynamic characteristics of arrays of wave power devices. Oceanogr Lit Rev 1998;9(45): 1712.
[57] Kagemoto H, Yue DK. Interactions among multiple three-dimensional bodies in water waves: an exact algebraic method. J Fluid Mech 1986;166:189–209.
[58] Child BFM. On the configuration of arrays of floating wave energy converters. Ph.D. thesis. The University of Edinburgh; 2011.
[59] Child B, Venugopal V. Optimal configurations of wave energy device arrays. Ocean Eng 2010;37(16):1402–17.
[60] Ruiz PM, Ferri F, Kofoed JP. Sensitivity analysis of wec array layout parameters effect on the power performance. In: Proceedings of the 11th European wave and tidal energy conference; 2015. Nantes.
[61] McNatt JC, Venugopal V, Forehand D. A novel method for deriving the diffraction transfer matrix and its application to multi-body interactions in water waves. Ocean Eng 2015;94:173–85.
[62] De Chowdhury S, Nader J-R, Sanchez AM, Fleming A, Winship B, Illesinghe S, Toffoli A, Babanin A, Penesis I, Manasseh R. A review of hydrodynamic investigations into arrays of ocean wave energy converters. 2015. arXiv preprint, 1508.00866.
[63] Folley M. Section iii - wave energy converter array modelling techniques. In: Folley M, editor. Numerical modelling of wave energy converters. Academic Press; 2016. p. 151–225. https://doi.org/10.1016/B978-0-12-803210-7.00010-4. http://www.sciencedirect.com/science/article/pii/B9780128032107000104.
[64] Poli P, Hersbach H, Dee DP, Berrisford P, Simmons AJ, Vitart F, Laloyaux P, Tan DG, Peubey C, Thépaut J-N, et al. ERA-20C: an atmospheric reanalysis of the twentieth century. J Clim 2016;29(11):4083–97.
[65] Berrisford P, Dee D, Fielding K, Fuentes M, Kallberg P, Kobayashi S, Uppala S. The ERA-interim archive. European Centre for Medium-Range Weather Forecasts; 2009.
[66] Hersbach H. The era5 atmospheric reanalysis. In: AGU fall meeting abstracts; 2016.
[67] Petersen GN. Meteorological buoy measurements in the Iceland Sea 2007-2009, supplement to: petersen, GN (2017): Meteorological buoy measurements in the Iceland Sea, 2007-2009. Earth Syst Sci Data 2017;9(2):779–89. https://doi.org/10.1594/PANGAEA.876206 10.5194/essd-9-779-2017.
[68] Mara FN. Irish marine Institute. 2018. Irish Government: https://www.marine.ie/Home/search/node/buoys.
[69] Duchon CE. Lanczos filtering in one and two dimens 1979;18:1016–22.
[70] Rogers JC. North Atlantic storm track variability and its association to the North Atlantic Oscillation and climate variability of northern Europe. J Clim 1997;10(7):1635–47. https://doi.org/10.1175/1520-0442(1997)010¡1635:NASTVA¿2.0.CO;2.
[71] Barnston AG, Livezey RE. Classification, seasonality and persistence of low-frequency atmospheric circulation patterns. Mon Weather Rev 1987;115:

1083–126.
[72] Thompson DWJ, Wallace JM. The arctic oscillation signature in the wintertime geopotential height and temperature fields. Geophys Res Lett 1998;25(9):1297–300. https://doi.org/10.1029/98GL00950.
[73] Cahill B, Lewis T. Wave period ratios and the calculation of wave power. In: 2nd marine energy technology symposium METS2014; 2014. Seattle, Wash.
[74] Taylor KE. Summarizing multiple aspects of model performance in a single diagram. J Geophys Res: Atmosphere 2001;106(D7):7183–92.
[75] Babarit A, Delhommeau G. Theoretical and numerical aspects of the open source BEM solver NEMOH. In: 11th European wave and tidal energy conference; 2015. p. 1–12. Nantes, France, EWTEC, no. 08C1.
[76] WAMIT Inc M. WAMIT v7.0 manual. 2013.
[77] Penalba M, Mérigaud A, Gilloteaux J-C, Ringwood JV. Influence of nonlinear froude–krylov forces on the performance of two wave energy points absorbers. J Ocean Eng Mar Energy 2017;3(3):209–20.
[78] Penalba M, Giorgi G, Ringwood JV. Mathematical modelling of wave energy converters: a review of nonlinear approaches. Renew Sustain Energy Rev 2017;78:1188–207.
[79] Penalba M, Ringwood JV. A high-fidelity wave-to-wire model for wave energy converters. Renew Energy 2019;134:367–78.
[80] Babarit A. A impact of long separating distances on the energy production of two interacting wave energy converters. Ocean Eng 2010;37:718–29.
[81] Ricci P, Saulnier J-B, Falcão A. Point-absorber arrays: a configuration study off the Portuguese west-coast. In: Proceedings of 7th European wave and tidal energy conference; 2007. p. 11–3. Porto, Portugal, September.
[82] REN21. Renewables 2019 global status report. Tech. Rep., ISBN 978-3-9818911-7-1. REN 21
[83] ICES. Tech. rep.. International Council for the Exploration of the SEA (ICES); Apr. 2017. https://doi.org/10.17895/ices.pub.3107. http://www.ices.dk/sites/pub/Publication%20Reports/Advice/2017/2017/Ecosystem_overview-Icelandic_Waters_ecoregion.pdf.
[84] Carnegie wave energy. Jul. 2019. Available at: http://www.carnegiewave.com/. [Accessed July 2019].
[85] Borgarino B, Babarit A, Ferrant P. Impact of wave interactions effects on energy absorption in large arrays of wave energy converters. Ocean Eng 2012;47:79–88.
[86] Stratigaki V, Troch P, Stallard T, Forehand D, Kofoed JP, Folley M, Benoit M, Babarit A, Kirkegaard J. Wave basin experiments with large wave energy converter arrays to study interactions between the converters and effects on other users in the sea and the coastal area. Energies 2014;7(2):701–34.
[87] Sen PK. Estimates of the regression coefficient based on Kendall's tau. J Am Stat Assoc 1968;63(324):1379–89.
[88] Theil H. A rank-invariant method of linear and polynomial regression analysis, 3; confidence regions for the parameters of polynomial regression equations. Stichting Mathematisch Centrum. Statistische Afdeling 1950:1–16.
[89] Sáenz J, Rodríguez-Puebla C, Fernández J, Zubillaga J. Interpretation of interannual winter temperature variations over southwestern. Europe 2001;106(D18):20641–52.
[90] Stopa JE, Cheung KF, Tolman HL, Chawla A. Patterns and cycles in the climate forecast system reanalysis wind and wave data. Ocean Model 2013;70:207–20.
[91] Izaguirre C, Méndez FJ, Menéndez M, Losada IJ. Global extreme wave height variability based on satellite data. Geophys Res Lett 2011;38(10).
[92] Freund MB, Henley BJ, Karoly DJ, McGregor HV, Abram NJ, Dommenget D. Higher frequency of central pacific el niño events in recent decades relative to past centuries. Nat Geosci 2019;12(6):450–5. https://doi.org/10.1038/s41561-019-0353-3.
[93] Ramos V, Lopez M, Taveira-Pinto F, Rosa-Santos P. In uence of the wave climate seasonality on the performance of a wave energy converter: A case study. Energy 2017;35:303–16. https://doi.org/10.1016/j.energy.2017.06.080.